ACS APPLIED NANO MATERIALS

www.acsanm.org
Article

Intraluminal Gold Nanoparticle-Loaded Liposomes Enable High-Resolution Nanoscale Mapping of Intracellular Delivery Pathways

Filippo Testa,[⊥] Andrea Banfi,[⊥] Marco Giustra, Giulia Tomaino, Luisa Fiandra, Paul Verkade, Maria Giulia Bravi, Giovanni Maria Vanacore, Lucia Salvioni,* and Davide Prosperi*

Cite This: *ACS Appl. Nano Mater.* 2026, 9, 13681−13694
Read Online

ABSTRACT: Understanding how lipid nanocarriers behave inside cells is key to improving nucleic acid and protein therapies. However, direct visualization of intracellular trafficking mechanisms is challenging because liposomes possess low intrinsic electron density and highly dynamic and flexible structural features. In this study, we present Lipo-Gold, a hybrid nanosystem consisting of clinically relevant liposomes containing multiple intraluminal small gold nanoparticles (AuNPs) and demonstrate its utility for nanoscale-resolution investigation of intracellular delivery pathways. Using an optimized adaptation of a stepwise in situ reduction strategy, specifically tailored to a cholesterol-containing lipid formulation, we generated multiple nonspace-filling AuNPs (15−20 nm) within each vesicle without altering the bilayer structure, surface charge, or colloidal stability, and overall vesicle architecture. Comprehensive physicochemical characterization, including dynamic light scattering, nanoparticle tracking analysis, and transmission electron microscopy (TEM), along with cellular uptake investigations by flow cytometry and confocal microscopy, demonstrates that Lipo-Gold retains the same biological identity and cellular interaction profile as the corresponding unmodified liposomes. In HeLa cells, Lipo-Gold also exhibits similar uptake kinetics and intracellular trafficking behavior comparable to unloaded vesicles. The intraluminal AuNPs generate strong electron contrast, enabling direct visualization of intracellular nanoscale transport events, including endocytic uptake, vesicle maturation, and subcellular confinement. Correlative light-electron microscopy (CLEM) further enabled spatial overlap between fluorescent liposome signals and electron-dense AuNP clusters, providing a multimodal imaging platform with nanometric structural resolution. Across all examined sections, AuNPs remained confined to membrane-bound endosomal compartments, with no evidence of cytosolic dispersion, consistent with the expected behavior of anionic, nonfusogenic liposomes. By combining fluorescence tracking with high-resolution structural imaging while preserving native liposome-cell interactions, Lipo-Gold offers a valuable tool for investigating intracellular delivery barriers and for guiding the rational development of next-generation lipid-based therapeutics.

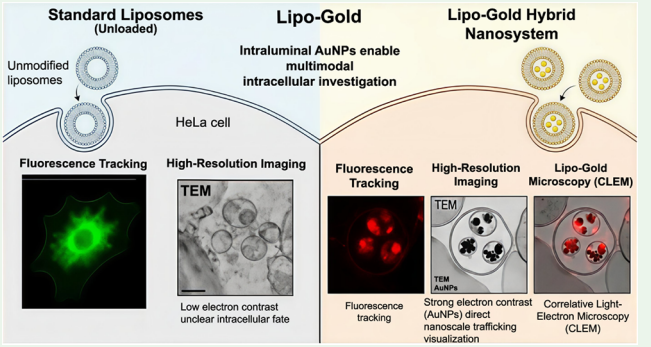

KEYWORDS: *liposomes, gold nanoparticles, hybrid nanocarriers, correlative light-electron microscopy, intracellular trafficking, endosomal escape, biointerfaces*

INTRODUCTION

Nanoparticles have been established as a promising drug delivery platform, offering the potential to overcome key pharmacokinetic and biodistribution limitations of conventional therapeutics. Among them, liposomes have attracted considerable interest due to their high biocompatibility, capacity for encapsulating both hydrophilic and hydrophobic molecules, and ease of surface functionalization. Several liposomal formulations have already reached clinical application, demonstrating their potential to improve therapeutic index and reduce off-target toxicity.[1] Despite these advantages, the ability to overcome biological barriers, particularly the cellular plasma membrane and endosomal compartments, remains a major bottleneck in the clinical translation of nanomedicines. While surface modification strategies have enabled improvements in circulation time and targeting efficiency, intracellular trafficking pathways and endosomal escape of nanoparticles remain inefficient and poorly understood for most nanocarriers, including liposomes.

Understanding how nanoparticles interact with and overcome these barriers is essential for the rational design of next-generation drug delivery systems. Previous studies took advantage of confocal imaging of subcellular structures (limited

Received: March 15, 2026
Revised: June 18, 2026
Accepted: June 24, 2026
Published: July 10, 2026

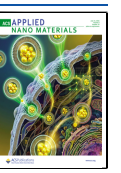

https://doi.org/10.1021/acsanm.6c01115
ACS Appl. Nano Mater. 2026, 9, 13681−13694

by low throughput and poor statistical significance),[2−5] assessment of biological responses to delivered materials, and detection of specific interactions between endogenous factors and exogenous cargo within defined cellular compartments.[6−8] However, investigating these mechanisms is particularly challenging for soft nanomaterials, including liposomes. Indeed, the elemental composition similarity between liposomes and cell membranes makes it difficult to distinguish them from endogenous biological structures with standard imaging techniques. Hybrid systems integrating gold nanoparticles with lipid membranes have been shown to preserve lipid architecture while imparting strong optical and plasmonic responses, enabling controlled drug release and advanced imaging functionalities.[9] Physical and biophysical methods are crucial for analyzing the mechanisms and efficiency of endosomal escape, serving as critical tools beyond functional readouts. The widely accessible calcein release assay (CRA) utilizes the self-quenching property of calcein at high concentrations.[10] Its dilution and subsequent fluorescence increase upon release into the neutral cytosol allows immediate evidence of cargo release. CRA analysis often employs confocal microscopy for spatial resolution, or flow cytometry to achieve high statistical power, though the latter lacks spatial resolution and can yield ambiguous results if nanocarriers alter cellular uptake. A major limitation of CRA is that the small calcein molecule may not accurately reflect the release profile of larger therapeutic cargos, such as nucleic acids or proteins. Similarly, cytosolic delivery of drug nanocarriers can be analyzed using FlAsH-EDT2 assay, which allows determining endosomal escape quantitatively.[8] However, also this method suffers from lack of intracellular point localization. To achieve nanometric detail, single-molecule localization microscopy (SMLM) offers unprecedented resolution essential for visualizing rare escape events of individual macromolecules (*e.g.*, mRNA).[11] Unfortunately, permeabilization processes required for immunostaining may compromise membrane integrity, introducing localization artifacts. For real-time kinetic insights into nanocarrier dynamics, single particle tracking (SPT) coupled with advanced deep learning analysis, such as DeepSPT, enables motion-to-function inference by classifying trajectories into biologically meaningful diffusion states.[12] DeepSPT rapidly and accurately segments heterogeneous motion, allowing the prediction of biological events solely based on diffusion, thereby minimizing the reliance on extensive multicolor labeling. Nevertheless, diffusion heterogeneity poses challenges for quantitative interpretation and often requires complementary biophysical validation. For rigorous mechanistic investigation, supported lipid bilayers combined with total internal reflection fluorescence (TIRF) microscopy isolate the role of electrostatics and pH in membrane interactions, enabling single lipid-nanoparticle resolution inspection of fusion kinetics and cargo fate at early endosomal membrane mimics.[13] However, this reductionist model cannot fully recapitulate the biochemical and structural complexity of native cell membranes. In addition, the split luciferase endosomal escape quantification (SLEEQ) assay enables highly sensitive, direct measurement of cytosolic delivery, reaching picomolar detection limits thanks to a complementation signal generated exclusively when the cargo reaches the cytosol.[14] Nonetheless, its wide applicability may be hindered by undesired constraints, including incompatibility with a range of pharmacological inhibitors and the need for specific cargo designs. Besides these method-dependent limitations, inherently low electron contrast, structural deformability, and rapid dynamics of liposomes further challenge their precise high-resolution localization and trafficking investigation. Fluorescent labeling strategies offer some insights but are often insufficient to capture the full picture of liposome behavior at the ultrastructural level. Moreover, fluorescent dyes can potentially alter the surface properties of nanoparticles or dissociate from the carrier, leading to misinterpretation of uptake and trafficking data.

To overcome the above restrictions, we developed a hybrid nanosystem, termed Lipo-Gold, in which a cluster of small gold nanoparticles (AuNPs) are synthesized *in situ* within the intraluminal space of conventional liposomes. The rationale behind the design of Lipo-Gold is to retain the biological and structural properties of liposomes during their interactions with cells, while leveraging the optical and electron-dense features of AuNPs to enable direct visualization and high-resolution tracking of liposome dynamics inside the cell. AuNPs are especially attractive for this purpose thanks to their well-defined plasmonic behavior, exceptional photostability, and strong contrast in electron microscopy. Similar gold-liposome nanocomposites − occasionally termed "golden liposomes" − have been exploited for photothermal triggering, multimodal imaging, and improved pharmacokinetics.[9,15,16] Importantly, incorporating AuNPs into the vesicle core preserves the native surface characteristics of the liposomes, preventing alterations that could otherwise affect their cellular interaction profile. In contrast, systems with AuNPs embedded in or coating the membrane can markedly alter bilayer rigidity, plasmonic coupling, and stimulus-responsive release profiles.[17,18] Consequently, Lipo-Gold are expected to represent a faithful surrogate for unmodified liposomes in biological assays. The Lipo-Gold system enables the use of advanced optical and electron microscopy techniques to study liposome-cell interactions with greater spatial and temporal resolution. Related Lipo-Gold and magnetic-plasmonic vesicle hybrids have been engineered as theranostic probes, enabling photoacoustic or optoacoustic tumor imaging and photothermal therapy.[19,20] It also provides a model system to investigate the mechanisms of cellular uptake and intracellular trafficking of liposomes, including their possible entrapment in endosomal compartments and the propensity to escape the endosome. Analogous biomineralization-inspired strategies use protein nanocages such as ferritin, apoferritin fibrils, albumin particles, or viral capsids to direct the in situ growth or encapsulation of metal nanoparticles (*e.g.*, Au, Ag, CuS, Au@Ag), yielding highly defined hybrid theranostic platforms.[21,22]

In this work, we report on the synthesis, characterization, and biological evaluation of Lipo-Gold as a model platform for studying the interaction of liposomes with cells. We showed that the inclusion of AuNPs in the vesicle core did not alter the physicochemical properties nor the biological behavior of the nanocarrier. Using a combination of fluorescence labeling, flow cytometry, confocal microscopy, transmission electron microscopy (TEM), and correlative light-electron microscopy (CLEM),[23] we demonstrated that Lipo-Gold faithfully mimics the uptake and intracellular fate of unlabeled liposomes, while enabling direct visualization and tracking of its subcellular localization in a cancer cell model of interest, i.e., the human cervical epithelial adenocarcinoma (HeLa).

https://doi.org/10.1021/acsanm.6c01115
ACS Appl. Nano Mater. 2026, 9, 13681−13694

EXPERIMENTAL SECTION

Cell Culture

HeLa cells were cultured in Dulbecco's Modified Eagle's Medium (DMEM) supplemented with 10% fetal bovine serum (FBS), 2 mM L-glutamine, penicillin (50 U/mL) and streptomycin (50 μg/mL). Cells were maintained at 37 °C in humidified atmosphere containing 5% CO_2 and subcultured prior to confluence using trypsin-EDTA. Cells were regularly tested for mycoplasma, and all experiments were performed on mycoplasma-free cells. All reagents were purchased by Euroclone.

Statistical Analysis

Data were reported as mean ± SD (standard deviation) or median ± SD. The differences among groups were determined by either one-way ANOVA or two-way ANOVA followed by the Tukey's post-test: (*) $p < 0.05$, (**) $p < 0.01$, (***) $p < 0.005$, (****) $p < 0.001$. A p-value of less than 0.05 was considered significant. Statistical analyses were performed using GraphPad Prism version 10.6.1 (GraphPad Software, San Diego, CA, USA).

Liposome Synthesis

Dipalmitoylphosphatidylcholine (DPPC, Avanti Research), cholesterol, 1,2-distearoyl-*sn*-glycero-3-phosphoethanolamine-*N*-[methoxy-(polyethylene glycol)-2000] (DSPE-PEG-OCH_3, Avanti Research) and 1,2-distearoyl-*sn*-glycero-3-phosphoethanolamine-*N*-[carboxy-(polyethylene glycol)-2000] (DSPE-PEG-COOH, Avanti Research) were dissolved in chloroform at a molar ratio of 62:33:4:1, placed in a round-bottom flask and the solvent was evaporated by rotary evaporator. The thin lipid film was hydrated overnight with 0.3 M AA solution (1 mL, final lipid concentration 25 mM) in ultrapure water under shaking. The mixture was then placed in an ultrasonic water bath set at 60 °C for 2.5 h and then sonicated for 45 min to fully resuspend lipids. Lipid vesicles were sequentially extruded through 800, 200, and 100 nm polycarbonate (PC) membranes (Whatman, UK) using a Mini-Extruder kit (Avanti Research) at 60 °C. Nonencapsulated AA was removed by dialysis, performed by placing 800 μL of liposome solution in a GeBAflex Midi 3.5 kDa Tube (Gene Bio-Application Ltd., Israel), against of ultrapure water (1 L). Dialysis was performed overnight at 4 °C, then water was replaced, and dialysis was performed additionally for 6 h at 4 °C. Finally, liposome nanoparticles were recovered and kept at 4 °C. For DiD'-labeled nanoparticle formulation, DiD' was added to the lipid mixture prior to film formation to yield DPPC:cholesterol:DSPE-PEG-OCH_3:DSPE-PEG-COOH:DiD' = 60.7:32.5:3.9:0.98:1.96 molar ratio. The final labeling concentration was set at 2% (mol:mol ratio) relative to total lipid content to ensure strong fluorescence intensity without affecting membrane stability.

Lipo-Gold Synthesis

Lipo-Gold was synthesized by addition of $HAuCl_4$ to AA encapsulating liposomes, performed at room temperature after dialysis purification. $HAuCl_4$ was prepared at 50 mM in ultrapure water and added to Lipo sample to reach final concentrations, ranging from 0.5 to 5 mM. After each addition, nanoparticles were immediately vortexed for 10 s and the formation of AuNPs and AA saturation were monitored by UV/vis spectroscopy. For this, Lipo and Lipo-Gold were diluted 50-fold in ultrapure water in UV cuvettes (Sarstedt, Germany) and analyzed using a Nanodrop 2000c spectrophotometer (Thermofisher Scientific, US).

Encapsulated Ascorbic Acid Quantification

A theoretical calculation of total encapsulated AA was carried out, considering the AA concentration in the aqueous compartment of Lipo as identical to the concentration of the outside solution. This assumption is based on the absence of a driving force for the encapsulation of AA, and a negligible leak of AA from Lipo during dialysis, as the lipidic bilayer holds little fluidity at 4 °C. The calculation is based on the average diameter of Lipo, as measured by nanoparticle tracking analysis, and the concentration of AA employed for the synthesis of Lipo. Internal diameter was calculated as the total diameter minus 10 nm to account for the thickness of double-sided lipid bilayer. The total internal area and volume were calculated assuming spherical shape as $4/3\pi r^3$, and a conversion factor of 10−18 was used to convert nm^3 to mm^3, corresponding to μL. Finally, total μmol of encapsulated AA were calculated from internal volume and molar concentration of AA. Direct quantification of encapsulated AA was performed with a modified 3-(4,5-dimethylthiazol-2-yl)-5-(3-carboxymethoxyphenyl)-2-(4-sulfophenyl)-2H-tetrazolium (MTS) assay. Lipo and Lipo-Gold (100 μL, 100, 500, or 1000 times diluted in ultrapure water) together with standard samples of known AA concentration were placed in 96-well plate (Costar, Corning). MTS (20 μL) was added to each well and samples were incubated at 37 °C for 15 min. Following incubation, 490 nm absorbance of each well was recorded with an EnSight multimode plate reader (PerkinElmer, US). A calibration curve was determined from standard samples correlating 490 nm absorbance to AA concentrations. A linear regression fit was used to determine the AA concentrations of Lipo and Lipo-Gold from the respective recorded absorbance. Total μmol of AA in samples was calculated considering dilution factor. Results were expressed as mean ± SD, n = 3 independent experiments.

Dynamic Light Scattering (DLS) Analysis

The nanoparticle hydrodynamic diameter and Zeta Potential (ZP) were analyzed by DLS using the Nano ZS Zetasizer (Malvern Instruments Ltd. Worcestershire, UK) operating at a light source wavelength of 633 nm and a fixed scattering angle of 173°. Samples were diluted in ultrapure water, maintaining attenuator values between 8 and 10. Results were expressed as mean ± SD of 3 independent measurements.

Nanoparticle Tracking Analysis (NTA)

Nanoparticle size distributions were characterized using NanoSight NS300 (Malvern Co., UK) equipped with a 488 nm laser excitation source and high sensitivity scientific CMOS camera. NTA 3.0 was used for data collection and analysis. Samples were diluted in 0.22 μm-filtered ultrapure water and manually injected into the sample chamber using 1 mL plastic syringes. All video captures and analysis settings, including camera shutter, camera gain and detection threshold, remained identical for all samples. The results were expressed as mean ± SE (standard error) of 5 independent measurements, with acquisition time of 50 s each.

Transmission Electron Microscopy (TEM)

The morphology of NPs was observed on a Jeol JEM 2100Plus (Jeol, Japan) electron microscope, operating with an acceleration voltage of 200 kV and equipped with a 9 MP complementary metal oxide superconductor (CMOS) Gatan Rio9 digital camera (Gatan, Inc., US). The samples were diluted in ultrapure water and prepared by evaporating 5 μL onto 200-mesh carbon-coated copper grid (Ted Pella, US) and allowing it to dry on air. When contrast staining was needed, samples were stained with Uranyl Acetate Replacement (UAR) (Electron Microscopy Sciences, EMS) following manufacturer's instructions.

Cytotoxicity Assay

Cell viability after incubation with Lipo and Lipo-Gold was assessed by a cell proliferation kit based on tetrazolium salt (MTS) (Promega, US). HeLa cells were seeded in a 96-well plate (Costar, Corning) at a density of 5,000 cells/well in 100 μL of complete medium. On the following day, the medium was replaced with 100 μL of fresh complete medium containing Lipo or Lipo-Gold at different concentrations: 1, 5, 10, 25, 50, 100, 125, 250, and 500 μg/mL (referred to total lipid content). The cells were then incubated for 6, 24, and 48 h at 37 °C. At the end of the incubation, nanoparticles containing medium was removed and replaced with 100 μL of fresh medium, then 20 μL of the MTS reagent were added in each well and the plates were placed in an incubator for 3 h. The intensity of the colored reduced product of MTS was measured at 490 nm with an EnSight multimode plate reader (PerkinElmer, US). Cellular viability was expressed as % compared to an untreated cells sample, which was

https://doi.org/10.1021/acsanm.6c01115
ACS Appl. Nano Mater. 2026, 9, 13681−13694

set at 100%. Results were expressed as mean ± SD of 4 independent measurements.

Flow Cytometry Uptake Analysis

The uptake of labeled DiD'-Lipo and DiD'-Lipo-Gold in HeLa cells was evaluated by flow cytometry. Cells were seeded in a 12-well plate (Costar, Corning) (150,000 cells/well) and allowed to recover ON. Then, cells were incubated with DiD'-Lipo and DiD'-Lipo-Gold at concentrations of 0.1, 1, and 10 μg/mL (total lipid concentration) for 3 h. At the end of the incubation time, nanoparticle-containing medium was removed, and cells were rinsed twice with phosphate buffer saline (PBS) w/o Ca^{2+} and Mg^{2+} and detached with trypsin. Cells were collected in flow cytometry tubes and washed with PBS. Finally, the cell pellet was resuspended in PBS-EDTA 1%, and the cells were analyzed by flow cytometry with a Gallios Flow Cytometer (Beckman Coulter Inc.). For flow cytometry analysis, the excitation wavelength used was at 633 nm and the red fluorescence was collected through the band-pass of 660/20 nm. Cellular uptake was expressed as median red fluorescence intensity of a sample, normalized against untreated cell sample set at 1. Results are expressed as mean ± SD of 3 independent measurements.

Microscopy Internalization Analysis

The internalization of labeled DiD'-Lipo and DiD'-Lipo-Gold in HeLa cells was evaluated by epifluorescence microscopy. Borosilicate 1.5 cover glasses (Marienfeld, Germany) were inserted into a 12-well plate (Costar, Corning) and HeLa cells were seeded on top (150,000 cells/mL) and allowed to recover ON. Then, cells were incubated with DiD'-Lipo and DiD'-Lipo-Gold at concentrations of 0.5, 1, and 10 μg/mL (total lipid concentration) for 3 h. At the end of the incubation time, nanoparticle-containing medium was removed, and cells were washed twice with cold PBS w/o Ca^{2+} and Mg^{2+} and fixed with 4% paraformaldehyde (PFA) (Solarbio Science Technology Co) for 15 min at room temperature (0.5 mL/well). Fixed cells were washed with PBS and a blocking passage with 0.5 mL of PBS-BSA 0.2% solution in each well for 30 min at room temperature was carried out. Then, the cover glasses were detached from the wells and incubated with Rat anti-CD44 antibody (BioRad, US), by placing the cover glasses onto a 35 μL drop of antibody for 1 h at room temperature. The cover glasses were then placed in clean 12-well plates and washed twice with PBS. An identical procedure was followed for staining with AlexaFluor-555-conjugated Goat anti-Rat secondary antibody. Cell nuclei were stained with Hoechst 33342 diluted in PBS for 5 min at room temperature and cells were washed with cold PBS. Finally, cover glasses were placed on glass microscope slides with a drop of FluorSave mounting medium and images were acquired by a Leica THUNDER Imager Live Cell and 3D Assay (Leica, USA). Small Volume Computational Clearing (SVCC) from Leica was employed for fluorescence imaging. Blue, Yellow and Red fluorescence were excited respectively with a 395, 555, and 635 nm LED lasers and analyzed with 435/30, 594/32 and 695/58 band-pass filters. For semiquantitative analysis, a binary mask was generated by manual segmentation of cells based on plasma membrane yellow fluorescence using ImageJ (NIH, Bethesda, MD, USA). The mask was then employed for the quantification of mean red fluorescence intensity of the internal region of cells. Results are expressed as mean ± SD of >50 imaged cells in each sample, normalized against untreated cell sample.

TEM Lipo-Gold Internalization

For high resolution imaging of Lipo-Gold internalization and subcellular localization, treated cells were processed and imaged through transmission electron microscopy (TEM), following a standard protocol. Briefly, $2x10^6$ HeLa cells were seeded in 60 mm dishes and allowed to recover overnight. Then, cells were incubated with Lipo-Gold at concentrations of 10 or 100 μg/mL for 1 or 3 h at 37 °C. At the end of the incubation, cells were washed with PBS, detached with trypsin, collected in 1.5 mL tubes and pelleted via centrifugation. The cell pellet was fixed with 4% PFA for 2 h at room temperature and postfixed in 2.5% glutaraldehyde (GA) for 30 min at room temperature. Then, the tubes were cut with a razor, and the pellet was carefully detached from the bottom of the tube with a needle, avoiding disaggregation. The pellet was cut in smaller pieces, washed in cacodylate buffer and dehydrated via incubation in ethanol gradient at increasing concentrations. Each piece of pellet was incubated in ethanol 50%, 70%, 90% and 100%, with 3 consecutive steps of 10 min incubation in each solution. Following dehydration, cells were stained with osmium tetroxide and uranyl acetate and infiltrated in epoxy resin and placed in flat embedding rubber molds. The resin was left to polymerize at 65 °C for 3 days, then the hardened samples were collected from the molds, trimmed and cut with an EM UC7 ultramicrotome (Leica) to obtain 70 nm thin slices. Slices were collected on TEM copper grids and imaged with a FEI 120 kV Tecnai G2 Spirit BioTWIN microscope operating at accelerating voltage of 120 kV. Additional nanoparticles and cells analysis were performed using a JEOL JEM 2100 thermionic microscope operating at 200 kV.

Correlative Light-Electron Microscopy (CLEM)

CLEM experiments were performed to simultaneously visualize the subcellular localization of the DiD'-labeled lipidic shell and the electron dense AuNPs. For this, VPS35-GFP HeLa cells were plated in appropriate gridded coverslip 35 mm dishes (300,000 cells/dish) (MatTek, P35G-1.5-14-CGRD) and allowed to recover overnight. Then, cells were incubated with DiD'-Lipo-Gold at concentrations of 10 and 100 μg/mL for 1 h. At the end of the incubation time, nanoparticles containing medium was removed and cells were washed twice with PBS w/o Ca^{2+} and Mg^{2+} and fixed with 4% PFA for 15 min at room temperature (1 mL/dish). Fixed cells were washed with PBS and cell nuclei were stained with Hoechst 3342 diluted in PBS for 5 min at room temperature. Finally, cells were washed with PBS and kept at 4 °C. Cells were imaged with a Leica TCS SP5-II CLSM. The location of imaged cells in respect to the gridded coverslip was noted. Following fluorescence imaging, PBS was removed and briefly rinsed with bidistilled water and immediately incubated with osmium tetroxide (1% in bidistilled water) and uranyl acetate (saturated solution in bidistilled water) each for 20 min at room temperature under shaking. Then, an ethanol gradient (70%, 80%, 90%, 96%, 100%) was performed to fully dehydrate cells, each passage for 5 min at room temperature under shaking. Finally, cells were infiltrated with epoxy resin for 30 min at 65 °C, then the resin was exchanged with fresh one and incubated at 65 °C for 3 days to fully polymerize. To detach the glass coverslip from the bottom of the dishes, those were dipped multiple times in hot water and liquid nitrogen to facilitate permeation of water between the dish and the glass coverslip. Next, a sharp razor was employed to fully remove the coverslip.[47] The hardened resin was visualized under a stereo microscope and the cells of interest previously imaged were traced back with the aid of the gridded pattern. The excess resin around those was trimmed and removed with a sharp razor. Finally, thin 70 nm or thick 250 nm cell slices were obtained with an EM UC7 ultramicrotome (Leica), placed on top of TEM copper grids and left to airdry ON. Cells were imaged under a Talos L120C TEM (ThermoFisher) operating at 120 kV.

RESULTS AND DISCUSSION

The clinical translation of lipid-based nanomedicines is still facing major hurdles despite their high biocompatibility and ability to carry a variety of substances.[24] Understanding how lipid-based nanocarriers engage with cellular membranes, traffic through endosomal compartments, and eventually release their cargo remains a key challenge for the rational design of next-generation drug delivery systems. However, the soft, electron-poor, and highly dynamic nature of liposomes has long limited researcher ability to study these processes directly at high spatial resolution.[25]

Particularly, intracellular trafficking pathways and the mechanism of endosomal escape has remained so far poorly understood and inefficiently studied for most liposomal nanocarriers.[26] Investigating these processes is puzzling

https://doi.org/10.1021/acsanm.6c01115
ACS Appl. Nano Mater. 2026, 9, 13681−13694

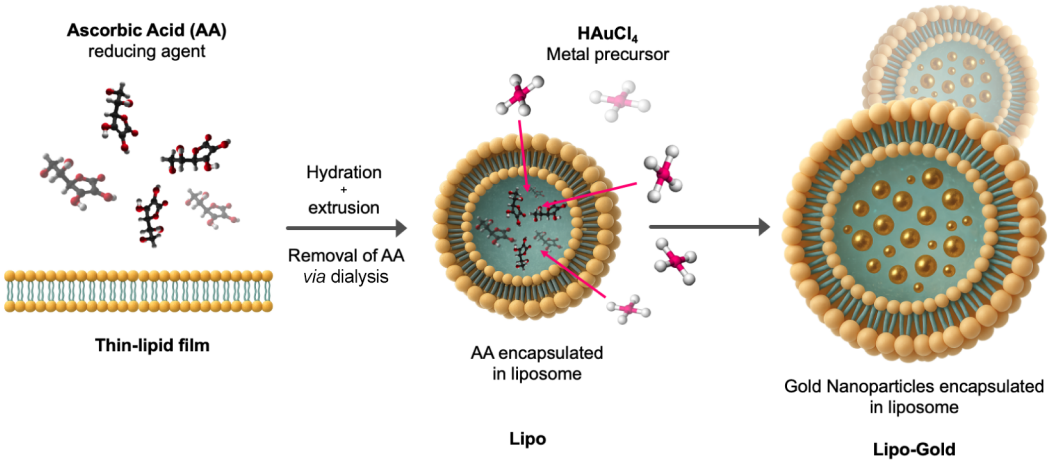

Figure 1. Schematic representation of Lipo and Lipo-Gold formulations. Liposomes encapsulating ascorbic acid (AA) were produced and purified. Gold nanoparticles (AuNPs) were synthesized by adding $HAuCl_4$ to the liposome suspension.

because soft nanomaterials like liposomes are similar in composition to native cell membranes, making them hard to visualize with standard imaging techniques. Furthermore, current advanced methods, such as SMLM and SPT, face limitations.[27,28] These include possible artifacts from membrane permeabilization, difficulties caused by diffusion variability, and the need for additional biophysical validation. In addition, although fluorescent labeling can offer insights, it may induce changes in the physical properties of the nanoparticles or cause them to dissociate from the carrier, which can lead to misinterpreting trafficking data.

To overcome these critical limitations, we developed a new hybrid nanoassembly called Lipo-Gold. This mixed organic–inorganic nanosystem was designed to retain the essential biological and chemical features of regular liposomes while using the electron-dense characteristics of AuNPs for clear, high-resolution visualization and tracking inside cells.

Synthesis and Characterization of Lipo-Gold Hybrid System

Lipo-Gold Synthesis. Motivated by the need for imaging-compatible nanosystems capable of directly elucidating how cells interact with lipid nanoparticles and vesicles, we engineered a hybrid nanostructure – termed Lipo-Gold – consisting of liposomes encapsulating AuNPs, specifically designed to circumvent the intrinsic limitations of conventional liposomes.[29−31] Lipo-Gold leveraged the native cell-interactive surface properties of liposomes and the strong optical and electron-dense characteristics of AuNPs. This design enabled the visualization and tracking of liposomes within cells with high spatial resolution without altering their surface chemistry through exogenous labeling. Conventional strategies for generating such hybrid architectures often rely on hydrating a dried lipid film with an aqueous suspension of presynthesized AuNPs, resulting in spontaneous liposome formation around some of the AuNPs. However, this passive encapsulation approach typically suffers from poor efficiency and heterogeneity, leading to a mixed population of empty liposomes, unencapsulated AuNPs, and a minority of hybrid vesicles.[32−34] To overcome these limitations and ensure the formation of a more homogeneous hybrid population, we optimized a bottom-up approach, in which AuNPs were synthesized in situ directly within the aqueous core of preformed liposomes, using the vesicle interior as a nanoreactor. This method provided spatial confinement of AuNPs within the liposomal lumen and preserved the external surface properties critical for cellular interaction. A lipid composition consisting of DPPC:Cholesterol:PEGylated DSPE (62:33:5 molar ratio) was selected based on clinically approved or trial-stage liposomal therapeutics. The mixture of saturated phospholipids and cholesterol offers enhanced stability to the vesicle, while PEGylation allows prolonged circulation and functionalization.[35] Building on a previously established protocol for liposomal/metallic nanohybrid synthesis, liposomes encapsulating the reducing agent ascorbic acid (AA) were produced via thin lipid film hydration followed by sonication and extrusion.[36] AA was chosen for its biocompatibility, strong reducing power and inability to cross the lipid membrane.[37,38] Residual AA was removed via dialysis at 4 °C to minimize the shear stress on the liposomal membrane and prevent AA leakage. AuNPs were synthesized by adding the metal precursor $HAuCl_4$ to the liposome suspension at room temperature, followed by vortex mixing. Lipo-Gold hybrids and control empty liposomes (Lipo) were stored at 4 °C and used for characterization and biological assay within 2 weeks. A schematic representation of the Lipo-Gold synthesis process is depicted in Figure 1.

Hybrid gold-liposome systems have increasingly attracted interest as multifunctional nanoplatforms combining the cargo-loading capacity and membrane mimicry of liposomes with the optical, plasmonic, and imaging properties of AuNPs. These systems have been explored for theranostics, photothermal therapy, triggered release, and multimodal imaging applications.[34]

Our synthetic approach used an optimized adaptation of the established intraluminal reduction strategy, originally reported by Lee et al.,[36] creating AuNPs in situ within the aqueous core of preformed liposomes and tailored here to a clinically relevant, cholesterol-containing lipid composition. This approach addressed the efficiency and variability issues normally found with passive encapsulation, ensuring that AuNPs remained confined within the vesicle luminal core while preserving the native surface chemistry of the liposomes essential for cell interaction. Conceptually, this confined in situ mineralization strategy parallels biomineralization-inspired approaches developed in protein nanocages such as ferritin, where metallic nanoparticles are synthesized within spatially

https://doi.org/10.1021/acsanm.6c01115
ACS Appl. Nano Mater. 2026, 9, 13681−13694

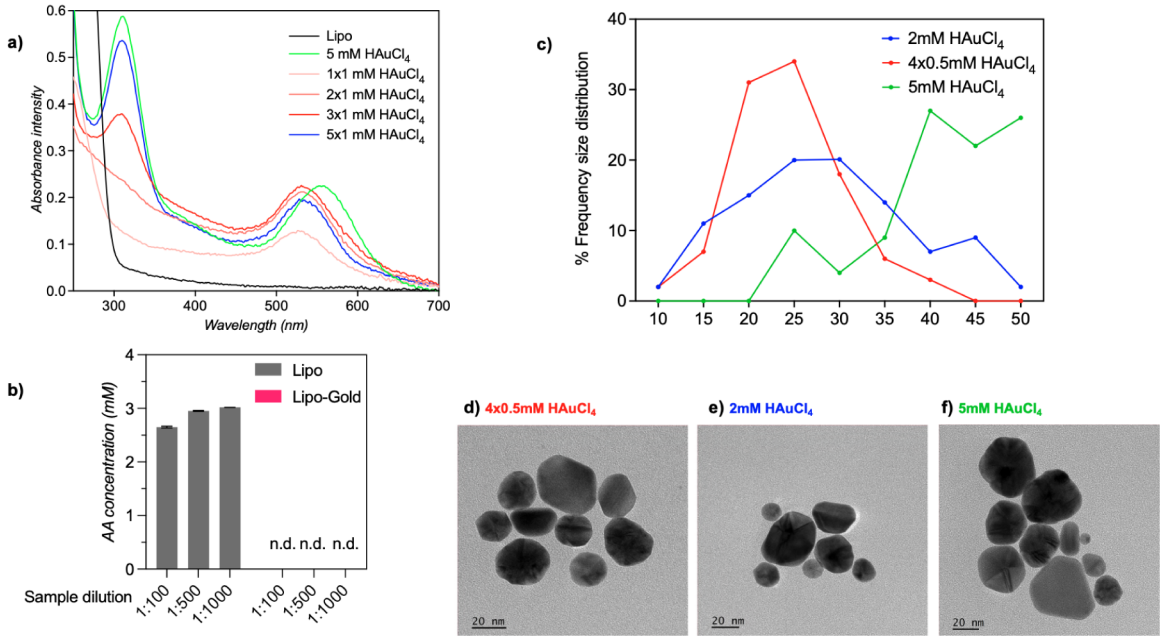

Figure 2. a) UV−vis analysis of AuNPs formation within liposomes. A characteristic plasmonic absorption band (∼530−560 nm) confirms the presence of AuNPs in Lipo-Gold samples, while it is absent in the liposome control. In samples with excess $HAuCl_4$, the nonreduced precursor shows a pronounced peak near 330 nm. b) AA quantification of Lipo and Lipo-Gold samples (n = 3) at three dilutions (1:100, 1:500, 1:1000). The assay measures MTS reduction, used here as an indirect measurement of the amount of AA contained within the samples. n.d. = not detectable c) Size-distribution frequency of AuNPs in Lipo-Gold samples prepared with different $HAuCl_4$ additions. Data represent the percentage of total particles measured in TEM images (n > 100 per condition). d−f) TEM images of Lipo-Gold nanoparticles showing the morphology of AuNPs obtained under three different synthesis conditions: d) 4 × 0.5 mM $HAuCl_4$, e) 2 mM $HAuCl_4$, f) 5 mM $HAuCl_4$. Scale bars as indicated.

restricted biological compartments to achieve controlled nucleation, stabilization, and preservation of the external biomolecular interface.[39] The careful step-by-step addition of $HAuCl_4$ up to 2 mM was crucial, resulting in a more uniform population of small AuNPs (15−30 nm), unlike methods that used a single step or oversaturation. Notably, our strategy produced multiple small AuNPs per vesicle, whereas earlier approaches frequently yielded a single, oversize particle occupying most of the liposomal lumen, which could increase membrane rigidity and compromise bilayer integrity.

Optimization of AuNPs Synthesis. The AuNPs synthesis conditions were optimized by varying $HAuCl_4$ concentration and the addition modality. UV−vis spectra (Figure 2a) showed that single-step addition of 5 mM $HAuCl_4$ (green line) generated a larger and polydisperse AuNP population, as evidenced by a broadened and red-shifted plasmonic peak. In contrast, stepwise addition of 1 mM $HAuCl_4$ aliquots produced a progressive increase in the plasmonic signal, reflecting ongoing AuNP formation. After the first addition (coral line), only a small peak was detectable at 530−560 nm, whereas a more intense and defined plasmonic band emerged after the second addition (orange line), consistent with efficient precursor reduction and continued AuNPs growth. Further additions no longer enhanced the plasmonic peak but instead increased absorption at ∼330 nm, corresponding to residual nonreduced $HAuCl_4$ accumulating under oversaturated conditions. Evidence that complete oxidation of AA occurred upon reaching approximately 2 mM $HAuCl_4$ was provided by quantifying the encapsulated AA content by two complementary approaches: (i) a theoretical estimation based on particle size and number, and (ii) a direct measurement using the commercially available reagent MTS, which upon reduction is converted into a water-soluble, colored formazan product. Since no specific driving force promotes AA encapsulation during the vesicle formation, it was assumed that equivalent AA concentrations were maintained inside the aqueous core of liposome as compared to the hydration buffer. Based on the internal diameter of individual liposomes and the total particle count determined by NTA, the total amount of encapsulated AA after dialysis was estimated to be approximately 3 mM (see Table S1 in the Supporting Information). AA levels were then quantified using the MTS reduction assay. A calibration curve (see Figure S1 in the Supporting Information) was generated using AA standards from 3 to 60 μM and used to determine AA levels in appropriately diluted samples. In Lipo, the AA content was calculated to be on average ∼2.9 mM, in agreement with the theoretical estimation. Moreover, since the assay relies on AA's reducing capacity, this result also suggested that liposomal confinement efficiently preserved AA from degradation and/or oxidation during the synthesis. In contrast, in Lipo-Gold obtained after stepwise addition of $HAuCl_4$ up to 2 mM, the AA was undetectable (Figure 2b), confirming complete oxidation upon AuNP formation. The saturation at ∼2 mM $HAuCl_4$ aligned with the stoichiometric electron transfer: each fully oxidized AA molecule releases 2 electrons, whereas Au(III) reduction to Au(0) requires 3 electrons. Thus, 3 mM AA would theoretically provide 6 mM electrons, sufficient to fully reduce 2 mM $HAuCl_4$. Collectively, these findings corroborate the hypothesis that AuNP formation reached completion at ∼2 mM $HAuCl_4$ due to total AA oxidation. Further analyses were conducted to confirm the impact of stepwise vs single-step addition of $HAuCl_4$ on AuNP size distribution. TEM was used to characterize the resulting AuNP populations in Lipo-Gold obtained by adding 2 mM $HAuCl_4$ in one step, Lipo-Gold produced with 5 mM $HAuCl_4$ to mimic oversaturation

https://doi.org/10.1021/acsanm.6c01115
ACS Appl. Nano Mater. 2026, 9, 13681−13694

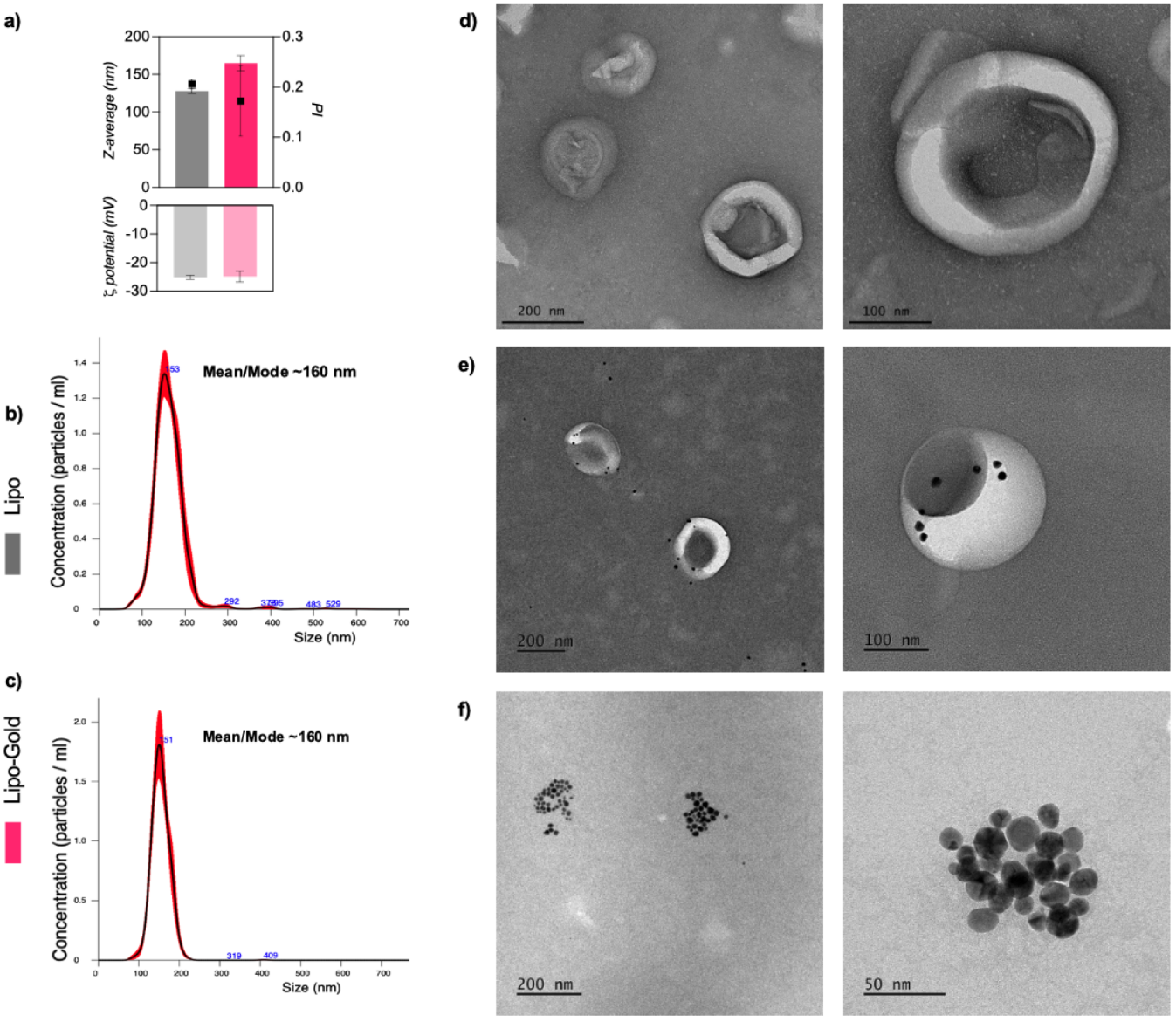

Figure 3. Physicochemical characterization of Lipo and Lipo-Gold nanoparticles. a) DLS analysis showing the Z-average hydrodynamic diameter, polydispersity index, and ZP, reported as the mean of three independent measurements. b) NTA size distribution of Lipo, obtained from five measurements and analyzed using FTLA (Finite Track Length Adjustment), a fitting method that corrects for particle trajectory truncation and provides a more accurate estimation of the modal particle size. c) NTA size distribution of Lipo-Gold nanoparticles based on five measurements and processed with FTLA fitting. d) Representative TEM images of UAR-stained Lipo highlighting vesicle morphology. e) TEM images of Lipo-Gold after UAR staining, showing both the lipid structure and the associated gold nanoparticles. f) TEM images of Lipo-Gold without UAR staining, where contrast arises primarily from the gold cores.

conditions, and Lipo-Gold prepared by adding 2 mM $HAuCl_4$ in four stepwise additions. Our data demonstrated that stepwise addition of $HAuCl_4$ yielded a more homogeneous and monodisperse AuNP population, with an average size in the range 15−30 nm (Figure 2c,d). In contrast, single-step addition of 2 mM $HAuCl_4$ resulted in a broader size distribution (15−45 nm) (Figure 2c,e), while excess precursor (5 mM) led to formation of larger AuNPs (Figure 2c,f). No AuNP formation was observed in the control sample lacking lipids (data not shown) but processed under identical synthetic and purification conditions, indicating that nonencapsulated AA is efficiently removed during purification. This supports the conclusion that AuNPs were generated specifically within the aqueous core of the liposomes. Notably, previously reported methods for in-liposome AuNPs synthesis typically resulted in particles approaching the full size of the internal aqueous cavity,[36] potentially compromising liposomal membrane integrity and surface properties, eventually jeopardizing the natural plasticity of the vesicle membrane.[40] In contrast, our strategy yielded multiple smaller AuNPs, which are far less likely to disrupt the structural integrity of the liposomal bilayer. Based on these results, the synthetic protocol for Lipo-Gold used for all subsequent experiment was standardized to four stepwise $HAuCl_4$ addition approach up to a final concentration of 2 mM metal precursor, ensuring controlled particle growth and size and improving the sample monodispersity. Under the selected experimental conditions, complete reduction of the added gold was achieved. Consequently, the Lipo-Gold formulation did not require any postsynthesis purification steps, and the gold content per unit lipid mass was estimated to

https://doi.org/10.1021/acsanm.6c01115
ACS Appl. Nano Mater. 2026, 9, 13681−13694

be 21.8 μg Au/mg lipids. This value was confirmed by ICP-OES analysis, which measured a gold content of 23.1 ± 3.2 μg Au/mg lipids (n = 3), in excellent agreement with the theoretical value.

More broadly, AuNP-membrane composite architectures have previously demonstrated that nanoscale gold incorporation can modulate membrane mechanics, improve structural stability, and enable advanced optical or optoacoustic functionalities while preserving biologically relevant membrane behavior.[9,34] In this context, the generation of multiple small intraluminal AuNPs rather than a single oversize metallic core may represent an advantageous strategy to minimize perturbation of bilayer dynamics while maintaining strong electron contrast.

Characterization of Lipo and Lipo-Gold. Lipo and Lipo-Gold were characterized in terms of morphology, size distribution, and surface charge using TEM, DLS, and NTA measurements. Both Lipo and Lipo-Gold exhibited hydrodynamic diameters ranging from 130 to 160 nm with polydispersity indices (PI) between 0.1 and 0.2 and surface charges of approximately −25 mV (Figure 3a). These results confirmed that both formulations maintained colloidal stability, with no significant aggregation, indicating that the AuNP synthesis process did not notably alter the liposomal properties. NTA analysis further corroborated these findings, displaying a sharp monomodal size distribution with both median and mode diameters around 160 nm for both Lipo and Lipo-Gold (Figure 3b,c and Table S2 in the Supporting Information). NTA was also utilized to quantify the concentration of nanoparticles in each sample (NPs/mL), previously employed in the theoretical estimation of encapsulated AA content. Morphological analysis via TEM provided additional insights into the structural characteristics of the nanosystems. AuNPs were visualized without staining due to their high electron density, whereas liposomes required contrast enhancement through UAR. Empty Lipo appeared as spherical vesicles with diameters generally ranging from 100 to 300 nm (Figure 3d). This apparent increase in size relative to DLS and NTA measurements is consistent with literature reports, as the dehydration process during TEM sample preparation can induce morphological alterations in soft nanoparticles. Lipo-Gold images, with (Figure 3e) or without UAR staining (Figure 3f), showed AuNPs with diameters of ∼20 nm, often multiple per vesicle, confirming that $HAuCl_4$ addition to preformed liposomes facilitated multiple nucleation events within a single liposomal core. Approximately 90% (analysis on 20 images) of AuNPs colocalized with liposomal structures; the minor fraction of apparently free AuNPs likely reflects both dehydration- and osmotic stress-induced membrane rupture during sample preparation. As a control, a physical mixture of empty liposomes and preformed AuNPs of comparable size was prepared and analyzed by TEM. In contrast to Lipo-Gold, the physical mixture showed no evidence of compartmentalization, with AuNPs randomly distributed in the extravesicular space and not structurally integrated with the liposomal vesicles (Figure S2).

As a complementary qualitative assay, agarose gel electrophoresis was performed by comparing intact Lipo-Gold with disrupted Lipo-Gold. Disruption of the liposomal structure induced by Triton X-100 + heating treatment altered the migration profile of the AuNP-associated signal, confirming its structural integration within the vesicular formulation in intact Lipo-Gold. This assay provides additional evidence that the gold signal specifically originates from AuNPs confined within the liposomal population. The corresponding gel images are reported in the Supporting Information (Figure S3).

It is acknowledged that cryo-TEM, which preserves the hydrated native state of liposomes, would provide the definitive ultrastructural confirmation of intraluminal AuNP localization; this will be pursued in future work. The convergent evidence provided above, including the complete removal of the extravesicular reductant by dialysis, the consistent intraluminal appearance of AuNPs in unstained TEM, and the gel electrophoresis retention behavior, collectively supports intraluminal localization in the interim.

Comprehensive physicochemical characterization confirmed the success of our design. Indeed, Lipo-Gold proved to maintain its chemical stability and exhibited hydrodynamic sizes (130−160 nm), polydispersity indices (0.1−0.2), and surface charges (around −25 mV) similar to those of control empty liposomes (Lipo). Our data supported the assumption that adding AuNPs did not appreciably alter the fundamental physical properties of the liposomal carrier.

A remaining point to consider is that, although the in situ synthesis strategy strongly improves the likelihood of generating AuNP-containing vesicles compared with passive AuNP encapsulation methods, the presence of a residual fraction of empty liposomes cannot be fully excluded. This limitation is intrinsic to the analysis of soft liposomal systems, for which separating empty from AuNP-loaded vesicles may perturb the formulation and alter the physicochemical properties of the objects subsequently used in biological experiments. Importantly, the main objective of this study was not to obtain a quantitatively purified population of AuNP-loaded liposomes, but rather to establish Lipo-Gold as a biologically faithful imaging probe in which intraluminal AuNPs act as electron-dense reporters for the AuNP-containing liposomal population. In this context, the comparable size distribution, surface charge, colloidal behavior, and cellular uptake profile of Lipo and Lipo-Gold support the suitability of the nonseparated formulation for intracellular trafficking studies.

Lipo-Gold Stability. Consistently with experimental time frame, storage stability studies confirmed that Lipo-Gold retained its size distribution and AuNP-associated SPR signal in ultrapure water at 4 °C for up to 14 days. In addition, Lipo-Gold maintained plasmonic stability after incubation in complete cell culture medium at 37 °C for up to 6 h, supporting its suitability for the short-term biological experiments performed in this study. Full stability data are reported in the Supporting Information (Figures S4, S5).

Cellular Uptake Studies

Cell Viability upon Treatment with Lipo-Gold. Prior to the evaluation of Lipo-Gold cellular uptake and intracellular detection, the tolerability of Lipo and Lipo-Gold was assessed using a cell viability assay on HeLa cells, selected for their extensive characterization and widespread use in nanoparticle-cell interaction studies. As shown in Figure S6 of the Supporting Information, both formulations were tolerated by the cells up to 100 μg/mL, allowing us to define the concentration range suitable for subsequent uptake experiments and for optimizing nanoparticle detection.

Assessment of Lipo-Gold Membrane Integrity. To investigate liposome-cell interactions using the Lipo-Gold nanosystem, it was first necessary to demonstrate that neither

https://doi.org/10.1021/acsanm.6c01115
ACS Appl. Nano Mater. 2026, 9, 13681−13694

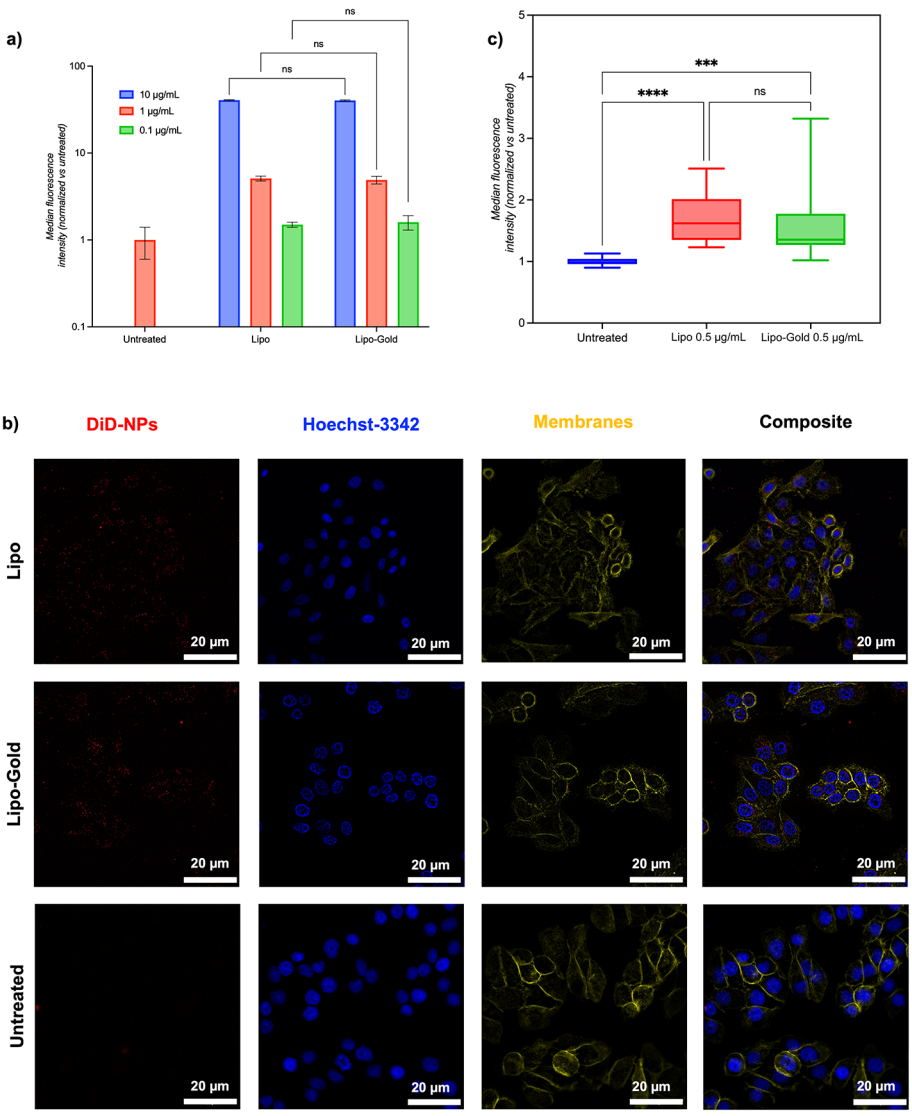

Figure 4. Cellular uptake of DiD'-Lipo and DiD'-Lipo-Gold. a) Uptake analyzed by flow cytometry. Data are shown as median fluorescence intensity (MFI) normalized to untreated cells (n = 3; ns = not significant). b) Representative images of separate channels: blue (nuclei), yellow (plasma membrane), and red (DiD'-labeled nanoparticles) for untreated cells and cells incubated with DiD'-Lipo or DiD'-Lipo-Gold (1 μg/mL, 3 h). c) Quantification of mean red fluorescence intensity in treated cells, normalized to untreated controls. Statistical significance: ns = not significant, *** = $p < 0.005$, **** = $p < 0.001$ (n = ~50).

the presence of encapsulated AuNPs nor the overall synthetic protocol caused alterations in the surface or in the biological properties of liposomal carrier. Although liposome structural organization is generally governed by their membrane composition and surface features, the presence of inorganic nanoparticles inside the soft lipid bilayer envelope can, under certain conditions, affect their mechanical properties or even their morphology.[41] In our system, however, AuNPs were low-density, and predominantly organized as a discrete distribution of small nanoparticles within each vesicle − a condition under which such mechanical side effects were not estimated to arise. To rigorously confirm such expectation, we employed fluorescence-based techniques, flow cytometry and fluorescence microscopy, which offer sensitive and quantitative analysis of nanoparticle uptake and intracellular distribution. To allow for direct comparison of Lipo and Lipo-Gold, both formulations were fluorescently labeled with a carbocyanine dye, the DiD' (1,1′-Dioctadecyl-3,3,3′,3′-tetramethylindodicarbocyanine, 4-chlorobenzenesulfonate). DiD' was selected for its ability to intercalate within the lipid bilayer without altering surface characteristics, thereby preserving the native biological behavior of the liposome while enabling reliable fluorescence-based detection and analysis. To assess the impact of fluorescent labeling on nanoparticle properties, DiD'-labeled formulations were subjected to physicochemical characterization as previously described. No appreciable differences were observed between labeled and unlabeled samples in terms of hydrodynamic diameter, ZP, polydispersity index (PDI), or size distribution profiles (see Figure S7 and Table S3 in the Supporting Information).

Flow Cytometry Uptake Analysis. HeLa cells were incubated with DiD'-Lipo and DiD'-Lipo-Gold at concentrations ranging from 0.1 to 10 μg/mL (lipid content) for 3 h. Following incubation, cells were washed to remove unbound nanoparticles and subsequently analyzed by flow cytometry. To account for intrinsic cell autofluorescence, the median fluorescence intensity of each sample was normalized to that of untreated cells. Both DiD'-Lipo and DiD'-Lipo-Gold exhibited

https://doi.org/10.1021/acsanm.6c01115
ACS Appl. Nano Mater. 2026, 9, 13681−13694

a dose-dependent increase in cellular fluorescence signal, indicating efficient nanoparticle-cell interactions (Figure 4a). Importantly, no significant differences were observed between the two formulations at any tested concentration, confirming that the presence of encapsulated AuNPs does not affect the surface-mediated interaction or uptake behavior of the liposomal carriers.

Fluorescence Microscopy Internalization Analysis. Since flow cytometry provides a quantitative assessment of nanoparticle-cell association but does not distinguish between membrane-bound and internalized materials, fluorescence microscopy was employed to gain deeper insight into cellular localization. DiD'-Lipo and DiD'-Lipo-Gold were tracked via fluorescence microscopy using a THUNDER imaging system. HeLa cells were incubated with DiD'-Lipo or DiD'-Lipo-Gold at 0.5 μg/mL (lipid content) for 3 h. THUNDER microscopy images (Figure 4b) showed blue-stained nuclei, yellow-labeled plasma membranes, and red fluorescence corresponding to DiD'-labeled nanoparticles. No background signal was detected in untreated control samples. Notably, cells treated with DiD'-Lipo and DiD'-Lipo-Gold displayed comparable levels of intracellular red fluorescence, confirming similar internalization efficiency. Additionally, red fluorescence appeared as punctate cytoplasmic spots rather than a diffuse signal, likely indicating nanoparticle localization within endolysosomal compartments. To further confirm the similar level of internalization of DiD'-Lipo and DiD'-Lipo-Gold, a semiquantitative fluorescence intensity analysis was performed (n = ~50). Binary masks were generated to define intracellular regions and mean red fluorescence intensity was measured and normalized to untreated controls. Fluorescence intensities for both DiD'-Lipo and DiD'-Lipo-Gold-treated cells were significantly elevated yet statistically indistinguishable (Figure 4c). Taken together, these findings confirmed that the incorporation of AuNPs within the liposomal aqueous core did not influence cellular interaction or internalization. These results validated Lipo-Gold as a robust model system for tracking and studying the biological fate of unlabeled liposomes.

Biological assays in HeLa cells established Lipo-Gold as an accurate model for studying the behavior of unlabeled liposomes. Initial tolerance tests showed that both Lipo and Lipo-Gold were suitable for uptake experiments at concentrations up to 100 μg/mL. Follow-up quantitative flow cytometry analysis of DiD'-labeled formulations demonstrated that the amount of cellular uptake increased with the dose in both DiD'-Lipo and DiD'-Lipo-Gold at all tested concentrations. This confirmed that the AuNPs did not interfere with the surface interactions or overall cellular uptake efficiency. Fluorescence microscopy supported these findings, showing similar internalization rates and subcellular localization characterized by punctate spots in the cytoplasm, which were consistent with entrapment in endolysosomal compartments.

Electron Microscopy Analysis. After confirming the comparable behavior of Lipo and Lipo-Gold using conventional fluorescence-based techniques, we further investigated the detailed cellular internalization and subcellular localization of label-free Lipo-Gold in HeLa cells, exploiting solely the unique properties of the encapsulated AuNPs by TEM. Cells were incubated with Lipo-Gold at 100 μg/mL (lipid content) for either 30 min or 1 h at 37 °C. At the first time point, AuNPs appeared as distinct electron-dense clusters, with individual nanoparticle size of approximately 15−20 nm. These clusters were confined within intracellular vesicles consistent with early endosomes, frequently localized close to the plasma membrane (Figure 5a). TEM imaging of cells after 1 h

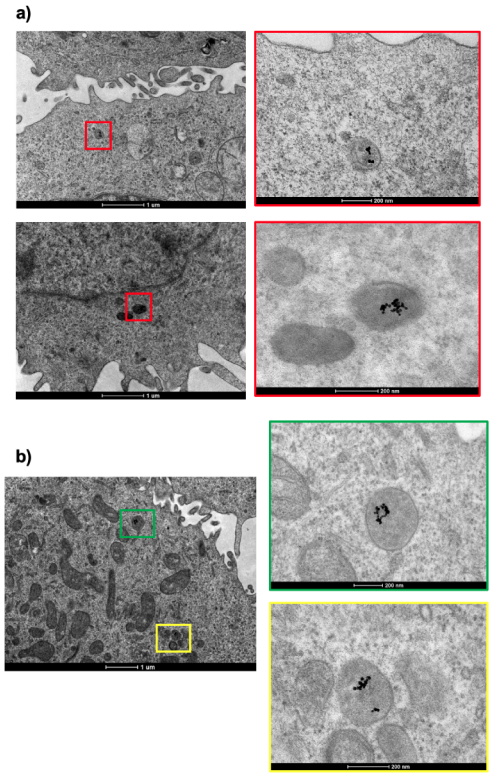

Figure 5. HeLa cells incubated with 100 μg/mL Lipo-Gold for 30 min (a) and 1 h (b). Thin slices (70 nm width) were cut and imaged under TEM, revealing the presence of AuNPs in endosomal-like structures, located beneath the plasma membrane at 30 min and deeper in the cytosol at 1 h.

incubation yielded consistent findings (Figure 5b): AuNPs again appeared in clustered assemblies of ~15−20 nm particles. However, the vesicular structures containing the nanoparticles were observed deeper into the cytoplasm and displayed larger diameters (~250−400 nm), compared to the ~200 nm vesicles observed at 30 min time point. These morphological differences indicate endosomal maturation, consistent with the progression from early endosomes to late endosomes or lysosomes. This interpretation is consistent with prior reports on the endocytic trafficking of liposomal nanocarriers.[42] Across all examined sections, AuNPs were consistently confined to membrane-bound compartments, with no evidence of free cytosolic dispersion, thereby ruling out endosomal escape processes. This result was somewhat expected, given the use of anionic liposomes lacking endosomal escape-promoting functionalities. Nonetheless, due to the ultrathin nature of TEM sections, possible rare cytosolic events could not be detected. Importantly, these findings support the suitability of Lipo-Gold as a model nanocarrier for dynamic TEM-based approaches aimed at elucidating the nanoparticle-cell interactions. The distinct spatial confinement of AuNPs within endosomal compartments enhances their contrast and traceability under electron microscopy, making Lipo-Gold an ideal candidate for future development and validation of advanced dynamic imaging methodologies.

https://doi.org/10.1021/acsanm.6c01115
ACS Appl. Nano Mater. 2026, 9, 13681−13694

Importantly, the high atomic density of AuNPs allowed us to study the subcellular fate of label-free Lipo-Gold using TEM. TEM results provided clear evidence of intracellular movement consistent with endocytic pathways: AuNPs were observed within vesicular structures close to the plasma membrane at 30 min (indicating early endosomes) and in larger vesicles deeper in the cytoplasm at 1 h (suggesting progression to late endosomes or lysosomes). Throughout all sections examined, AuNPs remained within membrane-bound compartments, indicating minimal free cytosolic dispersion or endosomal escape. This observation matched the expected behavior of the anionic liposome composition, which lacked specific features that promote endosomal escape. A key advantage of the TEM-based readout is that it enables direct morphological assignment of the containing compartment based on vesicle diameter, without requiring additional organelle markers: the size progression from ∼200 nm vesicles at 30 min to ∼250−400 nm at 1 h is consistent with endosomal maturation and could not be inferred from fluorescence data alone. Furthermore, unlike lipid-intercalated fluorescent dyes that track the carrier membrane, the intraluminal AuNPs report on the fate of the encapsulated cargo space, providing information that is inaccessible to conventional liposome labeling strategies. It should be acknowledged, however, that thin-section TEM (70 nm slices) samples only a small fraction of the total cell volume; consequently, rare cytosolic escape events occurring below the statistical sampling threshold cannot be detected or formally excluded. The absence of free cytosolic AuNPs in the examined sections is therefore consistent with, but does not quantitatively constrain, the frequency of endosomal escape. Future studies employing volume electron microscopy approaches (*e.g.*, FIB-SEM or serial block-face SEM) coupled with Lipo-Gold would enable a more comprehensive volumetric analysis of AuNP subcellular distribution.

Correlative Light-Electron Microscopy Analysis. To gain deeper insight into the intracellular trafficking of both the liposomal carrier (DiD'-labeled liposomes) and the encapsulated cargo (AuNPs), a CLEM approach was explored. Experiments were performed using a CRISPR-Cas9-engineered HeLa cell line expressing a VPS35-GFP fusion. VPS35 is a key component of the retromer complex and serves as a marker of early endosomes.[43] VPS35-GFP HeLa cells were incubated with DiD'-Lipo-Gold at 100 μg/mL for 1 h, washed and processed for fluorescence imaging. Cells were fixed with 4% PFA, stained with Hoechst for nuclear labeling, and maintained at 4 °C in PBS prior to further imaging. Confocal fluorescence microscopy identified nuclei (blue), VPS35-GFP-positive early endosomes (green), and DiD'-Lipo-Gold (red) (Figure 6a). Notably, no colocalization was observed between DiD' (red) and VPS35-GFP (green) signals (Pearson's correlation coefficient = 0.11), supporting that Lipo-Gold is predominantly localized in late endosomes or lysosomes after 1 h incubation. TEM images of the same group of cells previously imaged by confocal microscopy were acquired at higher magnification to correlate the intracellular localization of AuNPs with the DiD' signal (Figure 6c). The apparent angular offset between the fluorescence and TEM panels arises from the acquisition geometry inherent to the CLEM workflow: confocal images are recorded with a user-defined stage orientation, whereas TEM sections are collected on grids in a fixed orientation; the two data sets are coregistered computationally using anatomical landmarks (nuclear shape and cell boundary). Clusters of electron-dense AuNPs were observed within vesicular compartments consistent with endosomal structures, spatially corresponding to the red DiD' puncta observed in fluorescence images. These results confirmed that Lipo-Gold nanoparticles remained compartmentalized within endosomal-like vesicles at 1 h postincubation. Importantly, the AuNPs were still found confined within the liposomes, and the vesicular localization supported a late-endosomal/lysosomal identity. It should be noted that the CLEM experiment shown here served as a proof-of-principle demonstration of multimodal colocalization rather than a statistically powered analysis of subcellular distribution, which was addressed at the population level by flow cytometry and fluorescence microscopy data (Figure 4). The inherently low throughput of the CLEM workflow − requiring confocal imaging, resin embedding, ultramicrotomy, and TEM relocalization of the exact same cell − precluded routine multicell statistical analysis at this stage. Due to the mismatch between confocal axial resolution (∼0.5 μm) and TEM section thickness (70 nm), not all fluorescence puncta observed at the confocal level could be correlated with AuNPs in TEM images.

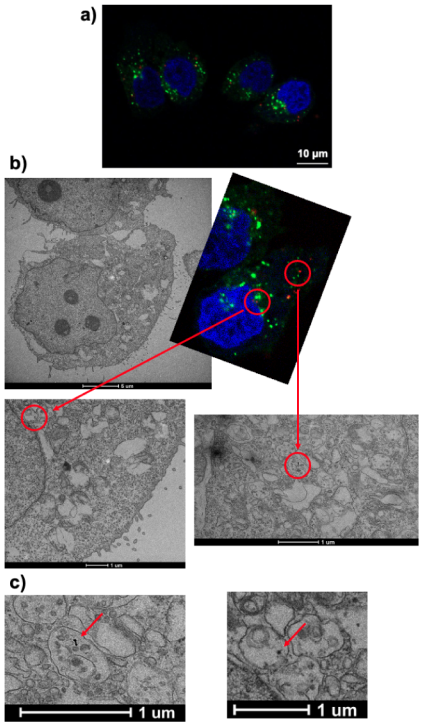

Figure 6. a) Confocal imaging of HeLa cells incubated with DiD'-Lipo-Gold for 1 h. Blue: nuclei; green: VPS35-GFP; red: DiD'-Lipo-Gold (single central slice from multiple 0.5 μm z-slices). b) Fluorescence and EM images of the cell of interest side by side, with correlation between red signal and presence of AuNPs in endosomal structures indicate by red circles. c) Higher-magnification images of the selected regions, highlighting AuNP-containing endosomal compartments corresponding to the fluorescence signal.

Eventually, CLEM[44] was utilized to investigate the use of a VPS35-GFP HeLa cell line as a marker for early endosomes to refine the subcellular localization. The lack of overlap between the DiD' fluorescence signal and the VPS35-GFP signal confirmed that Lipo-Gold was mostly localized in late endosomes or lysosomes after 1 h of incubation, validating the endosomal maturation noted in the standard TEM analysis. CLEM successfully linked the fluorescent puncta (representing

https://doi.org/10.1021/acsanm.6c01115
ACS Appl. Nano Mater. 2026, 9, 13681−13694

the liposomal structure) with the electron-dense clusters of AuNPs observed in vesicular compartments in the TEM images, confirming that the AuNPs remained restricted within the liposomes.

CONCLUSIONS

In summary, Lipo-Gold is a robust and versatile platform that retains the native biological profile of liposomes while addressing major technical challenges related to high-resolution imaging of soft nanomaterials. By integrating multiple intraluminal small AuNPs within clinically relevant liposomes, the platform enables direct nanoscale visualization and tracking through complementary optical and electron microscopy techniques, without perturbing membrane composition or colloidal behavior. This capability provides a powerful approach for nanoscale mapping of intracellular trafficking pathways and subcellular localization of lipid nanocarriers in biologically relevant environments. The key advantage of Lipo-Gold lies in the physical decoupling of the imaging probe from the carrier surface: because the AuNPs are confined within the aqueous lumen, the external lipid bilayer preserves its native physicochemical and biological properties, allowing faithful recapitulation of liposome−cell interactions while simultaneously providing strong electron contrast for subcellular localization. This combination of preserved biological behavior and enhanced nanometric-resolution visualization is difficult to achieve using conventional liposomal labeling strategies alone.

Beyond its role as a mechanistic probe, the implications of Lipo-Gold extend well beyond fundamental biointerface science. Our results supported the assumption that the integration of fusogenic lipids or peptides is needed to promote efficient cargo endosomal escape, a conclusion with important implications for the design of highly functional RNA delivery systems. Such advanced, imaging-competent hybrid liposomes could substantially accelerate the development of clinically relevant nanomedicines. Indeed, Lipo-Gold offers a direct, high-resolution readout of endosomal trafficking, enabling rapid identification of lipid compositions that optimize uptake, minimize lysosomal routing, or favor endosomal destabilization − features essential for RNA and protein therapeutics. Using Lipo-Gold also represents a route to derisk biologics delivery technologies, as it allows visualization of intracellular bottlenecks, including sequestration, aggregation, and failed escape, helping developers anticipate failure modes early and reducing attrition in the translation pipeline. Finally, because this hybrid system relies on clinically validated lipid compositions and gold species widely considered biocompatible, compatibility with manufacturing and regulatory paradigms is envisaged, supporting potential integration into scalable and GMP-suitable processes.

From a broader materials-design perspective, Lipo-Gold belongs to an emerging class of bioinspired hybrid nanosystems in which soft biological compartments guide the formation and spatial confinement of inorganic nanostructures. Similar concepts have been explored in ferritin-based nanoreactors and other biomolecular templates to combine structural precision, colloidal stability, and multifunctionality within a single nanoscale platform.[45,46]

The present study also establishes Lipo-Gold as a promising model platform for future dynamic-TEM investigations and advanced multimodal imaging approaches with high spatiotemporal resolution. In particular, it is well-suited for the development and validation of imaging methods that require high-contrast tracking aimed at clarifying nanocarrier internalization pathways, endosomal maturation processes, and rare intracellular delivery events such as endosomal escape in functionalized lipid formulations.

It is nonetheless worth pointing out that this technology has great scope for implementation, and several aspects deserve further investigation. Because the liposomes used here are anionic and nonfusogenic, their trafficking predominantly follows degradative endosomal pathways, limiting the observation of membrane destabilization and cytosolic release events. Future implementations of Lipo-Gold may incorporate pH-responsive lipids, fusogenic peptides, or even ionizable lipid compositions resembling clinically relevant lipid nanoparticles (*e.g.*, LNP-like formulations), thereby enabling direct visualization of the structural correlates associated with endosomal disruption and intracellular cargo release. Additionally, the current study was performed in HeLa cells, which provide a robust yet simplified experimental model; future work will therefore evaluate Lipo-Gold trafficking behavior in primary cells and in 3D tumor spheroids and organoids to better assess its translational relevance.

By enabling biologically faithful nanoscale imaging of lipid nanocarriers while maintaining native liposome−cell interactions, Lipo-Gold provides a valuable technological framework for investigating intracellular delivery barriers and for guiding the rational engineering of next-generation nanotherapeutic systems for biologic cargo delivery. Following these considerations, Lipo-Gold can reasonably be regarded not only as a mechanistic probe but also as a translational enabler, i.e., a platform that connects nanoscale biological insight into the design of safer, more effective nanocarriers capable of supporting the next wave of RNA, protein, and gene-delivery therapeutics.

ASSOCIATED CONTENT

Supporting Information

The Supporting Information is available free of charge at https://pubs.acs.org/doi/10.1021/acsanm.6c01115.

Table S1: theoretical estimation of encapsulated ascorbic acid (AA) content based on nanoparticle tracking analysis (NTA)-derived liposome concentration and size; Figure S1: calibration curve generated using ascorbic acid (AA) standards and measured by MTS assay at 490 nm; Figure S2: TEM image of a physical mixture of empty liposomes and preformed AuNPs of comparable size; Figure S3: agarose gel electrophoresis analysis of intact and disrupted Lipo-Gold; Figure S4: Lipo-Gold storage stability in ultrapure water at 4 °C for up to 14 days, evaluated by NTA and UV−vis spectroscopy; Figure S5: Lipo-Gold stability in complete cell culture medium at 37 °C for up to 24 h, evaluated by UV−vis spectroscopy; Table S2: mean and mode of size distribution curve, and concentration of Lipo and Lipo-Gold, measured by NTA; Figure S6: cell viability of HeLa cells incubated with increasing concentrations of Lipo and Lipo-Gold for 24 and 48 h; Figure S7: characterization of DiD'-labeled formulations via Dynamic Light Scattering (DLS) analysis; Table S3: mean and mode of size distribution curve, and concentration of DiD'-Lipo and DiD'-Lipo-Gold, measured by NTA (PDF)

https://doi.org/10.1021/acsanm.6c01115
ACS Appl. Nano Mater. 2026, 9, 13681−13694

AUTHOR INFORMATION

Corresponding Authors

Lucia Salvioni − *NanoBioLab, Department of Biotechnology and Biosciences, University of Milano-Bicocca, Milano 20126, Italy; Nanobiotechnologies for Health Center (NANOMIB), University of Milano-Bicocca, Vedano al Lambro 20854, Italy;* orcid.org/0000-0002-9385-5926; Email: lucia.salvioni@unimib.it

Davide Prosperi − *NanoBioLab, Department of Biotechnology and Biosciences, University of Milano-Bicocca, Milano 20126, Italy; Nanobiotechnologies for Health Center (NANOMIB), University of Milano-Bicocca, Vedano al Lambro 20854, Italy;* orcid.org/0000-0003-4577-9575; Email: davide.prosperi@unimib.it

Authors

Filippo Testa − *NanoBioLab, Department of Biotechnology and Biosciences, University of Milano-Bicocca, Milano 20126, Italy;* orcid.org/0000-0002-9234-7778

Andrea Banfi − *NanoBioLab, Department of Biotechnology and Biosciences, University of Milano-Bicocca, Milano 20126, Italy;* orcid.org/0009-0006-9918-3290

Marco Giustra − *NanoBioLab, Department of Biotechnology and Biosciences, University of Milano-Bicocca, Milano 20126, Italy; Nanobiotechnologies for Health Center (NANOMIB), University of Milano-Bicocca, Vedano al Lambro 20854, Italy;* orcid.org/0000-0002-9122-8515

Giulia Tomaino − *NanoBioLab, Department of Biotechnology and Biosciences, University of Milano-Bicocca, Milano 20126, Italy*

Luisa Fiandra − *NanoBioLab, Department of Biotechnology and Biosciences, University of Milano-Bicocca, Milano 20126, Italy; Nanobiotechnologies for Health Center (NANOMIB), University of Milano-Bicocca, Vedano al Lambro 20854, Italy;* orcid.org/0000-0002-7512-9752

Paul Verkade − *School of Biochemistry and Biomedical Sciences, University of Bristol, University Walk, Bristol BS8 1TD, U.K.;* orcid.org/0000-0002-2497-1026

Maria Giulia Bravi − *LUMiNaD, Department of Materials Science, University of Milano-Bicocca, Milano 20126, Italy*

Giovanni Maria Vanacore − *LUMiNaD, Department of Materials Science, University of Milano-Bicocca, Milano 20126, Italy;* orcid.org/0000-0002-7228-7982

Complete contact information is available at: https://pubs.acs.org/10.1021/acsanm.6c01115

Author Contributions

⊥F.T. and A.B. contributed equally to this work. All authors have given approval to the final version of the manuscript. D.P., L.F., and G.M.V. conceived the project. F.T., L.S., and D.P. designed the experiments and wrote the manuscript. A.B. contributed to the manuscript writing. F.T. performed the majority of the experiments and analyzed the data. A.B., G.T., and M.G. helped with nanomaterials and cellular experiments and with data analysis. M.G.B. helped with TEM experiments. A.B. and L.S. prepared the figures. P.V. supervised CLEM experiments. P.V. and G.M.V. helped with CLEM data analyses. D.P. and L.S. conceptualized and supervised the project, guided the experimental design and data analysis. L.F., P.V., G.M.V., D.P., and L.S. revised the final manuscript.

Notes

The authors declare no competing financial interest.

ACKNOWLEDGMENTS

The authors are grateful to Tiziano Catelani for help with TEM image acquisition. This work was supported by the SMART-electron project that has received funding from the European Union's Horizon 2020 Research and Innovation Program under Grant Agreement No. 964591.

REFERENCES

(1) Agrawal, S. S.; Baliga, V.; Londhe, V. Y. Liposomal Formulations: A Recent Update. *Pharmaceutics* **2025**, *17*, 36.

(2) Munson, M. J.; O'Driscoll, G.; Silva, A. M.; Lázaro-Ibáñez, E.; Gallud, A.; Wilson, J. T.; Collén, A.; Esbjörner, E. K.; Sabirsh, A. A High-Throughput Galectin-9 Imaging Assay for Quantifying Nanoparticle Uptake, Endosomal Escape and Functional RNA Delivery. *Commun. Biol* **2021**, *4*, 211.

(3) Vermeulen, L. M. P.; Brans, T.; Samal, S. K.; Dubruel, P.; Demeester, J.; De Smedt, S. C.; Remaut, K.; Braeckmans, K. Endosomal Size and Membrane Leakiness Influence Proton Sponge-Based Rupture of Endosomal Vesicles. *ACS Nano* **2018**, *12*, 2332−2345.

(4) Wang, T. Y.; Sun, Y.; Muthukrishnan, N.; Erazo-Oliveras, A.; Najjar, K.; Pellois, J. P. Membrane Oxidation Enables the Cytosolic Entry of Polyarginine Cell-Penetrating Peptides. *J. Biol. Chem* **2016**, *291*, 7902−7914.

(5) Kosuge, M.; Takeuchi, T.; Nakase, I.; Jones, A. T.; Futaki, S. Cellular Internalization and Distribution of Arginine-Rich Peptides as a Function of Extracellular Peptide Concentration, Serum, and Plasma Membrane Associated Proteoglycans. *Bioconjugate Chem* **2008**, *19*, 656−664.

(6) Lönn, P.; Kacsinta, A. D.; Cui, X.-S.; Hamil, A. S.; Kaulich, M.; Gogoi, K.; Dowdy, S. F. Enhancing Endosomal Escape for Intracellular Delivery of Macromolecular Biologic Therapeutics. *Sci. Rep* **2016**, *6*, 32301.

(7) Verdurmen, W. P. R.; Mazlami, M.; Plückthun, A. A Quantitative Comparison of Cytosolic Delivery Via Different Protein Uptake Systems. *Sci. Rep* **2017**, *7*, 13194.

(8) Rotem, R.; Bertolini, J. A.; Salvioni, L.; Barbieri, L.; Rizzuto, M. A.; Tinelli, V.; Gori, A.; Adams, S.; Colombo, M.; Prosperi, D. Direct Quantification of Cytosolic Delivery of Drug Nanocarriers Using FlAsH-EDT2. *Nanomedicine* **2023**, *47*, 102626.

(9) Caselli, L.; Paolini, L.; Fong, W.; Montis, C.; Zendrini, A.; Cardellini, J.; Bergese, P.; Berti, D. The gold nanoparticle-lipid membrane synergy for nanomedical applications. *Nanoscale Horiz* **2025**, *10*, 1863−1881.

(10) Hausig-Punke, F.; Richter, F.; Hoernke, M.; Brendel, J. C.; Traeger, A. Tracking the Endosomal Escape: A Closer Look at Calcein and Related Reporters. *Macromol. Biosci* **2022**, *22*, No. e2200167.

(11) Paramasivam, P.; Franke, C.; Stöter, M.; Höijer, A.; Bartesaghi, S.; Sabirsh, A.; Lindfors, L.; Arteta, M. Y.; Dahlén, A.; Bak, A.; Andersson, S.; Kalaidzidis, Y.; Bickle, M.; Zerial, M. Endosomal Escape of Delivered mRNA from Endosomal Recycling Tubules Visualized at the Nanoscale. *J. Cell Biol* **2022**, *221*, No. e202110137.

(12) Kæstel-Hansen, J.; de Sautu, M.; Saminathan, A.; Scanavachi, G.; Bango Da Cunha Correia, R. F.; Juma Nielsen, A.; Bleshøy, S. V.; Tsolakidis, K.; Boomsma, W.; Kirchhausen, T.; Hatzakis, N. S. Deep Learning-Assisted Analysis of Single-Particle Tracking for Automated Correlation Between Diffusion and Function. *Nat. Methods* **2025**, *22*, 1091−1100.

(13) Aliakbarinodehi, N.; Niederkofler, S.; Emilsson, G.; Parkkila, P.; Olsén, E.; Jing, Y.; Sjöberg, M.; Agnarsson, B.; Lindfors, L.; Höök, F. Time-Resolved Inspection of Ionizable Lipid-Facilitated Lipid Nanoparticle Disintegration and Cargo Release at an Early Endosomal Membrane Mimic. *ACS Nano* **2024**, *18*, 22989−23000.

(14) Teo, S. L. Y.; Rennick, J. J.; Yuen, D.; Al-Wassiti, H.; Johnston, A. P. R.; Pouton, C. W. Unravelling Cytosolic Delivery of Cell Penetrating Peptides with a Quantitative Endosomal Escape Assay. *Nat. Commun* **2021**, *12*, 3721.
(15) Cardellini, J.; Balestri, A.; Comparini, L.; Lonetti, B.; Brucale, M.; Valle, F.; Berti, D.; Montis, C. Controlling plasmonic supra-structures through self-assembly of gold nanoparticles with hybrid copolymer-lipid vesicles. *J. Colloid Interface Sci* **2024**, *654*, 848−858.
(16) Appidi, T.; Rajalakshmi, P. S.; Chinchulkar, S. A.; Pradhan, A.; Begum, H.; Shetty, V.; Srivastava, R.; Ganesan, P.; Rengan, A. K. A plasmon-enhanced fluorescent gold coated novel lipo-polymeric hybrid nanosystem: synthesis, characterization and application for imaging and photothermal therapy of breast cancer. *Nanoscale* **2022**, *14*, 9112−9123.
(17) Santhosh, P.; Tenev, T.; Šturm, L.; Ulrih, N.; Genova, J. Effects of Hydrophobic Gold Nanoparticles on Structure and Fluidity of SOPC Lipid Membranes. *Int. J. Mol. Sci* **2023**, *24*, 10226.
(18) Al-Ahmady, Z.; Donno, R.; Gennari, A.; Prestat, E.; Marotta, R.; Mironov, A.; Newman, L.; Lawrence, J.; Tirelli, N.; Ashford, M.; Kostarelos, K. Enhanced Intra-Liposomal Metallic Nanoparticle Payload Capacity Using Microfluidics Assisted Self-Assembly. *Langmuir* **2019**, *35* (41), 13318−13331.
(19) Cardellini, J.; Surpi, A.; Muzzi, B.; Pacciani, V.; Innocenti, C.; Sangregorio, C.; Dediu, V.; Montis, C.; Berti, D. Magnetic−Plasmonic Nanoscale Liposomes with Tunable Optical and Magnetic Properties for Combined Multimodal Imaging and Drug Delivery. *ACS Appl. Nano Mater* **2024**, *7*, 3668−3678.
(20) Zhuang, L.; Lian, Y.; Zhu, T. Multifunctional gold nano-particles: bridging detection, diagnosis, and targeted therapy in cancer. *Mol. Cancer* **2025**, *24*, 228.
(21) Mohanty, A.; Parida, A.; Raut, R.; Behera, R. Ferritin: A Promising Nanoreactor and Nanocarrier for Bionanotechnology. *ACS Bio Med Chem Au* **2022**, *2*, 258−281.
(22) Wang, Z.; Huang, P.; Jacobson, O.; Wang, Z.; Liu, Y.; Lin, L.; Lin, J.; Lu, N.; Zhang, H.; Tian, R.; Niu, G.; Liu, G.; Chen, X. Biomineralization-Inspired Synthesis of Copper Sulfide-Ferritin Nanocages as Cancer Theranostics. *ACS Nano* **2016**, *10*, 3453−3460.
(23) Shafiei, N.; Stähli, D.; Burger, D.; Di Fabrizio, M.; van den Heuvel, L.; Daraspe, J.; Böing, C.; Shahmoradian, S. H.; van de Berg, W. D. J.; Genoud, C.; Stahlberg, H.; Lewis, A. J. Correlative Light and Electron Microscopy for Human Brain and Other Biological Models. *Nat. Protoc* **2025**, *20*, 2994−3023.
(24) Sercombe, L.; Veerati, T.; Moheimani, F.; Wu, S. Y.; Sood, A. K.; Hua, S. Advances and Challenges of Liposome Assisted Drug Delivery. *Front. Pharmacol* **2015**, *6*, 286.
(25) Sahay, G.; Alakhova, D. Y.; Kabanov, A. V. Endocytosis of Nanomedicines. *J. Controlled Release* **2010**, *145*, 182−195.
(26) Allen, T. M.; Cullis, P. R. Liposomal Drug Delivery Systems: From Concept to Clinical Applications. *Adv. Drug Delivery Rev* **2013**, *65*, 36−48.
(27) Klein, T.; Proppert, S.; Sauer, M. Eight Years of Single-Molecule Localization Microscopy. *Histochem. Cell Biol* **2014**, *141*, 561−575.
(28) Simon, F.; Weiss, L. E.; van Teeffelen, S. A Guide to Single-Particle Tracking. *Nat. Rev. Methods Primers* **2024**, *4*, 66.
(29) Bian, X.; Luo, Z.; Peng, B.; Chen, J.; Lo, P. K.; Zhou, L.; Wen, Y. Engineered Bionanomaterials for Precision Delivery of Nucleic Acid Drugs. *Small* **2025**, *21*, No. e02667.
(30) Zahednezhad, F.; Allahyari, S.; Sarfraz, M.; Zakeri-Milani, P.; Feyzizadeh, M.; Valizadeh, H. Liposomal Drug Delivery Systems for Organ-Specific Cancer Targeting: Early Promises, Subsequent Problems, and Recent Breakthroughs. *Exp. Opin. Drug Delivery* **2024**, *21*, 1363−1384.
(31) Birnbaumer, G.; Kupcu, S.; Jungreuthmayer, C.; Richter, L.; Vorauer-Uhl, K.; Wagner, A.; Valenta, C.; Sleytr, U.; Ertl, P. Rapid liposome quality assessment using a lab-on-a-chip. *Lab Chip* **2011**, *11*, 2753−2762.
(32) Zhigaltsev, I. V.; Tam, Y. Y. C.; Kulkarni, J. A.; Cullis, P. R. Synthesis and characterization of hybrid lipid nanoparticles containing gold nanoparticles and a weak base drug. *Langmuir* **2022**, *38*, 7858−7866.
(33) Dichello, G. A.; Fukuda, T.; Maekawa, T.; Whitby, R. L. D.; Mikhalovsky, S. V.; Alavijeh, M.; Pannala, A. S.; Sarker, D. K. Preparation of Liposomes Containing Small Gold Nanoparticles Using Electrostatic Interactions. *Eur. J. Pharm. Sci* **2017**, *105*, 55−63.
(34) Idoudi, S.; Ismail, R.; Rachid, O.; Elhissi, A.; Alkilany, A. M. The golden liposomes: preparation and biomedical applications of gold-liposome nanocomposites. *J. Nanotheranostics* **2023**, *4*, 201−227.
(35) Liu, P.; Chen, G.; Zhang, J. A Review of Liposomes as a Drug Delivery System: Current Status of Approved Products, Regulatory Environments, and Future Perspectives. *Molecules* **2022**, *27*, 1372.
(36) Lee, J.-H.; Shin, Y.; Lee, W.; Whang, K.; Kim, D.; Lee, L. P.; Choi, J.-W.; Kang, T. General and Programmable Synthesis of Hybrid Liposome/Metal Nanoparticles. *Sci. Adv* **2016**, *2*, No. e1601838.
(37) Hannesschlaeger, C.; Pohl, P. Membrane Permeabilities of Ascorbic Acid and Ascorbate. *Biomolecules* **2018**, *8*, 73.
(38) Odehnalová, K.; Balouch, M.; Storchmannová, K.; Petrová, E.; Konefał, M.; Zadražil, A.; Berka, K.; Brus, J.; Štěpánek, F. Liposomal Copermeation Assay Reveals Unexpected Membrane Interactions of Commonly Prescribed Drugs. *Mol. Pharmaceutics* **2024**, *21*, 2673−2683.
(39) Zang, J.; Zheng, B.; Zhang, X.; Arosio, P.; Zhao, G. Design and Site-Directed Compartmentalization of Gold Nanoclusters within the Intrasubunit Interfaces of Ferritin Nanocage. *J. Nanobiotechnol* **2019**, *17*, 79.
(40) Zhao, C.; Li, L.; Wang, C.; Liu, X.; Deng, H. Ternary Nanoparticle Rigidity Regulates mRNA Vaccines Transportation. *Biomaterials* **2026**, *326*, 123628.
(41) Hui, Y.; Liu, Y.; Yang, G.; Weng, Y.; Hou, F.; Wang, X.; Fang, S.; Gao, H.; Zhao, C.-X. Critical role of nanomaterial mechanical properties in drug delivery, nanovaccines and beyond. *Adv. Mater* **2025**, *37*, No. e2413779.
(42) Wang, C.; Zhao, T.; Li, Y.; Huang, G.; White, M. A.; Gao, J. Investigation of Endosome and Lysosome Biology by Ultra pH-Sensitive Nanoprobes. *Adv. Drug Delivery Rev* **2017**, *113*, 87−96.
(43) Guo, Q.; Chen, K.-E.; Gimenez-Andres, M.; Jellett, A. P.; Gao, Y.; Simonetti, B.; Liu, M.; Danson, C. M.; Heesom, K. J.; Cullen, P. J.; et al. Structural basis for coupling of the WASH subunit FAM21 with the endosomal SNX27−Retromer complex. *Proc. Natl. Acad. Sci. U. S. A* **2024**, *121*, No. e2405041121.
(44) van den Dries, K.; Fransen, J.; Cambi, A. Fluorescence CLEM In Biology: Historic Developments and Current Super-Resolution Applications. *FEBS Lett* **2022**, *596*, 2486−2496.
(45) Moglia, I.; Santiago, M.; Arellano, A.; Salazar Sandoval, S.; Olivera-Nappa, Á.; Kogan, M. J.; Soler, M. Synthesis of dumbbell-like heteronanostructures encapsulated in ferritin protein: Towards multifunctional protein based opto-magnetic nanomaterials for biomedical theranostic. *Colloids Surf., B* **2025**, *245*, 114332.
(46) Lach, M.; Strelow, C.; Meyer, A.; Mews, A.; Beck, T. Encapsulation of Gold Nanoparticles into Redesigned Ferritin Nanocages for the Assembly of Binary Superlattices Composed of Fluorophores and Gold Nanoparticles. *ACS Appl. Mater. Interfaces* **2022**, *14* (8), 10656−10668.
(47) Mäntylä, E.; Verkade, P. Some Tips and Tricks for a Correlative Light Electron Microscopy Workflow Using Stable Expression of Fluorescent Proteins. *Methods Cell Biol* **2024**, *187*, 43−56.

https://doi.org/10.1021/acsanm.6c01115
ACS Appl. Nano Mater. 2026, 9, 13681−13694